



HAL
open science

Development of a split-window algorithm for estimating sea surface temperature from the Chinese Gaofen-5 data

Yuanyuan Chen, Si-Bo Duan, Jélila Labed, Zhao-Liang Li

► To cite this version:

Yuanyuan Chen, Si-Bo Duan, Jélila Labed, Zhao-Liang Li. Development of a split-window algorithm for estimating sea surface temperature from the Chinese Gaofen-5 data. *International Journal of Remote Sensing*, 2019, 40 (5-6), pp.1621-1639. 10.1080/01431161.2018.1488295 . hal-02377663

HAL Id: hal-02377663

<https://hal.science/hal-02377663>

Submitted on 8 Dec 2020

HAL is a multi-disciplinary open access archive for the deposit and dissemination of scientific research documents, whether they are published or not. The documents may come from teaching and research institutions in France or abroad, or from public or private research centers.

L'archive ouverte pluridisciplinaire **HAL**, est destinée au dépôt et à la diffusion de documents scientifiques de niveau recherche, publiés ou non, émanant des établissements d'enseignement et de recherche français ou étrangers, des laboratoires publics ou privés.

1 **Development of a split-window algorithm for estimating**
2 **sea surface temperature from the Chinese Gaofen-5 data**

3 Yuanyuan Chen^{1,2,3}, Si-Bo Duan¹, J éila Labeled³ and Zhao-Liang
4 Li^{1,3,*}

5 ¹ *Key Laboratory of Agricultural Remote Sensing, Ministry of*
6 *Agriculture/Institute of Agricultural Resources and Regional Planning,*
7 *Chinese Academy of Agricultural Sciences, Beijing, 100081, China*

8 ² *Key Laboratory of Cultivated Land Use, Ministry of Agriculture, P. R.*
9 *China; Chinese Academy of Agricultural Engineering, Beijing, 100121, China*

10 ³ *ICube, Uds, CNRS (UMR7357), 300 Bld Sebastien Brant, CS10413, 67412,*
11 *Illkirch, France*

12 *lizhaoliang@caas.cn
13

14

15

16

17

18

19

20

21

22

23

24

25

26

27

28 **Development of a split-window algorithm for estimating sea**
29 **surface temperature from the Chinese Gaofen-5 data**

30 **Abstract:** Sea surface temperature (SST) is an essential climate
31 variable that can be used to assess climate change. One kind of method
32 commonly used to estimate SST based on remote sensing measurements
33 is the split-window (SW) algorithm. However, the derivation of the
34 linear SW algorithm does not appear to reflect reality because some
35 assumptions and approximations were used. Moreover, the quadratic
36 SW equation cannot be interpreted theoretically although it maintains
37 the structure of the linear SW equation. The Gaofen-5 (GF-5) satellite
38 launch is planned for 2017. Focusing on exploring the mechanism of
39 the SW algorithm using GF-5 data, this study investigated the
40 assumptions and approximations used to derive the linear SW technique.
41 Two revised equations of these assumptions and approximations were
42 developed. Combining the revised equations, a nonlinear SW algorithm
43 was obtained that could be simplified to the quadratic equation.
44 Compared with previous research, this study focuses more on the
45 theoretical interpretation and improves our understanding of the semi-
46 empirical quadratic SW equation. The matchup dataset produced by the
47 European Organization for the Exploitation of Meteorological Satellites
48 (EUMETSAT) Ocean and Sea Ice Satellite Application Facility (OSI-
49 SAF) was used to validate the quadratic SW algorithm. A bias of -0.05
50 K and a RMSE of 0.53 K were obtained.

51 **Keywords:** Sea surface temperature; Split-window; Revision; GF-5;
52 Thermal infrared

53 **1. Introduction**

54 As an important parameter in the exchange of energy between the ocean and
55 the atmosphere, the sea surface temperature (SST) reflects both oceanic and

56 atmospheric variability on multiple temporal and spatial scales (Fisher 1958;
57 Liu and Minnett 2015). High-quality SST datasets are needed for many
58 applications, such as numerical weather prediction, ocean forecasting, and
59 climate change assessment (Pinaridi et al. 2003; Barnett et al. 1993; Chelton and
60 Wentz 2005; Donlon et al. 2007). Knowledge of the distribution of SST is also
61 useful for locating various species of fish (Simpson 1994). Such investigations
62 can be satisfied using satellite remote sensing data. However, accurate
63 determination of SST from satellite data is a difficult task because the at-sensor
64 measured radiances include the atmospheric absorption and emission (Liu et al.
65 2013). Thus, removal of the atmospheric effects is a key step in the accurate
66 retrieval of SST from remotely sensed data.

67 Despite the problem of atmospheric effects, retrieval of SST
68 information from space using thermal infrared (TIR) data began in 1970.
69 Anding and Kauth (1970) first demonstrated that the atmospheric effects can
70 be almost compensated for by simultaneously using the radiometric
71 measurements in two properly selected TIR bands. Prabhakara et al. (1974) first
72 suggested the general method of estimating SST from two TIR channel
73 measurements. Therefore, the split-window (SW) technique for estimating SST
74 was derived based on the previous works, with the general idea that the
75 atmospheric effects are proportional to the difference between the at-sensor
76 radiances measured simultaneously in two TIR channels (McMillin 1975;
77 Ulivieri et al. 1994; Coll and Caselles 1997; Rozenstein et al. 2014). For

78 nighttime retrieval, the channel near 3.7 μm is often used to improve the
79 accuracy of SST retrieval because it's a more transparent band, compared with
80 the bands centered at 11 and 12 μm (Barton 1983). However, there is significant
81 solar radiation at this wavelength that restricts the channel to be used for
82 daytime SST retrieval (McClain, Pichel, and Walton 1985; Petrenko et al. 2014).
83 Since then, a variety of methods based on the SW technique have been
84 developed and improved to retrieve SST and LST (land surface temperature)
85 (McClain, Pichel, and Walton 1985; Becker and Li 1990; Sobrino, Li, and Stoll
86 1993; Niclòs et al. 2007; Qian et al. 2016).

87 In the derivation of the SW technique, some assumptions and
88 approximations were made to obtain the SST. One assumption is the first-order
89 Taylor approximation of the Planck function (Prabhakara, Dalu, and Kunde
90 1974; Becker 1987). Another assumption is that the atmospheric equivalent
91 temperatures in the two adjacent TIR channels were the same ($T_{ai} = T_{aj}$)
92 (McMillin 1975; Sobrino, Coll, and Caselles 1991). Notably, there are certain
93 restrictions for these assumptions. As demonstrated in the literature (Sobrino,
94 Coll, and Caselles 1991; Becker 1987), the linear approximation of the Planck
95 function is generally accurate under the condition that T and T_i are close to each
96 other (T represents the atmospheric equivalent temperature or surface
97 temperature and T_i is the brightness temperature measured by the satellite).
98 However, it is difficult to meet this condition due to the strong variability of
99 global atmospheric conditions. In addition, the hypothesis $T_{ai} = T_{aj}$ does not

100 appear to reflect reality. Therefore, these assumptions and approximations must
101 be re-examined.

102 The Gaofen-5 (GF-5) satellite is expected to be launched in 2017. An
103 advantage of the multiple spectral-imager (MSI) onboard GF-5 satellite is the
104 high spatial resolution (40 meters for TIR channels). As a result, applications
105 of the TIR data from GF-5 are different from those of other sensors with coarser
106 spatial resolutions. For example, the high resolution SST data of GF-5 can be
107 used to monitor the thermal pollution produced by the nuclear power. Thus,
108 there is an urgent need to develop an algorithm that is suitable for retrieving
109 SST from GF-5/TIR data. In this paper, the investigation of the following
110 assumptions and approximations: 1) the linearization of the Planck function and
111 2) the atmospheric equivalent temperatures in two TIR channels, which were
112 assumed to be the same was undertaken based on the Chinese GF-5 data. We
113 aim to explore the mechanism of the SW algorithm further through revising
114 these assumptions and approximations. The paper is organized as follows:
115 Section 2 describes the data used in this study. The theoretical revision and
116 derivation of the SW technique, including revision of the linearization of the
117 Planck function, revision of the $T_{ai} = T_{aj}$ hypothesis and analysis of the
118 developed SW algorithm, are documented in Section 3. The effect of instrument
119 noise on SST retrieval and the algorithm validation are described in Section 4.
120 The discussion is given in Section 5. Finally, Section 6 presents the conclusions.

121 **2. Data**

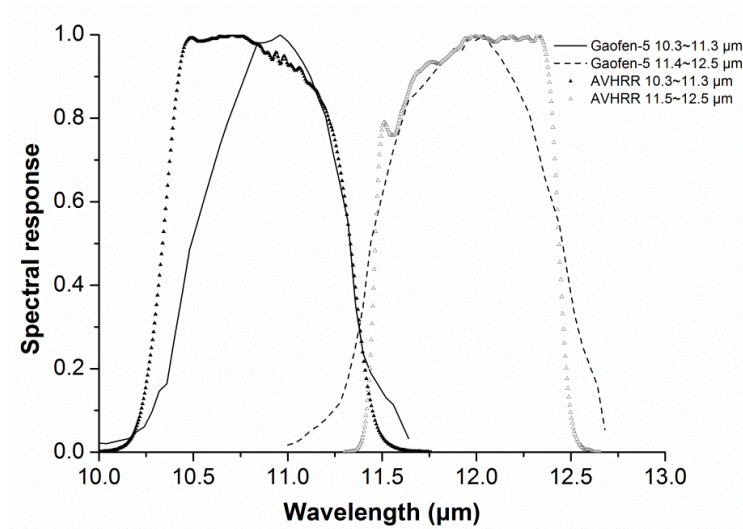
122 ***2.1 Chinese GF-5 data***

123 With the launch of the China High-resolution Earth Observation System
124 (CHEOS), China has entered a new era of high resolution operations. GF-5 is
125 the fifth satellite in a series of CHEOS, scheduled to be launched in 2017. One
126 of the major sensors onboard the GF-5 satellite is the multiple spectral-imager
127 (MSI) that includes 13 channels covering the spectral range from visible to TIR
128 and observes the earth almost at nadir. The channels centered at 10.8 μm and
129 11.95 μm are two TIR channels (labeled CH_{10.8} and CH_{11.95}, respectively,
130 hereafter) suitable for SW method, with a spatial resolution of 40 meters. The
131 spectral response functions of CH_{10.8} and CH_{11.95} are shown in Figure 1.

132 ***2.2 Matchup data set***

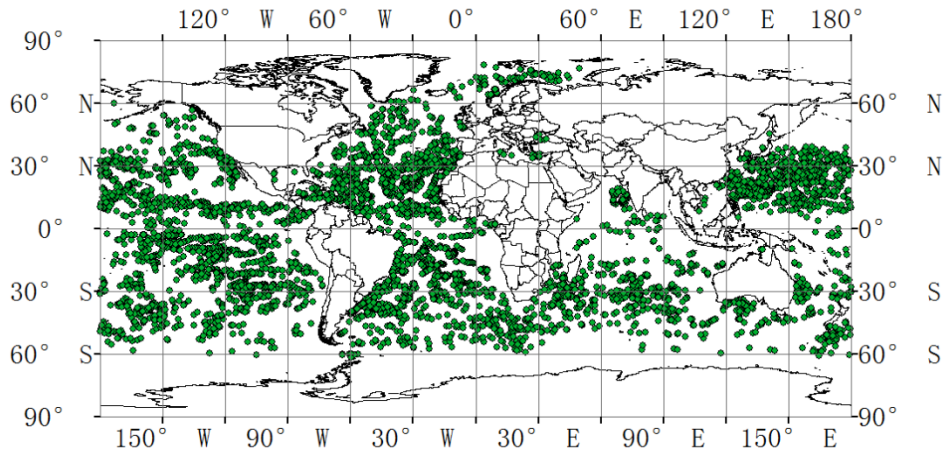
133 To assess the performance of the developed algorithm, Matchup dataset (MDS)
134 produced by the European Organization for the Exploitation of Meteorological
135 Satellites (EUMETSAT) Ocean and Sea-Ice Satellite Application Facility
136 (OSI-SAF) was collected. MDS was provided in NetCDF format, containing
137 the fields of latitude, longitude, viewing zenith angle (VZA), acquisition time,
138 AVHRR at-sensor brightness temperatures, in situ SSTs, etc. AVHRR
139 brightness temperatures are coincident in time and space with the in situ SSTs.
140 From Figure 1, which also displays the spectral response functions of AVHRR

141 SW channels, we can see that the spectral configuration of GF-5/MSI and
142 AVHRR SW channels is similar. Considering the lack of available GF-5 data
143 at present, the “true” GF-5 brightness temperature can be got from the AVHRR
144 measurements based on the relationship built by the simulated data for the
145 purpose of algorithm validation. The in situ SSTs recorded by drifting buoys
146 were collected from the Global Telecommunication System (GTS) with an
147 AVHRR pixel. Figure 2 shows the location distribution of in situ SSTs,
148 indicating the almost global coverage of in situ measurement.



149

150 Figure 1. Spectral response functions for Gaofen-5 and AVHRR split-window
151 channels.



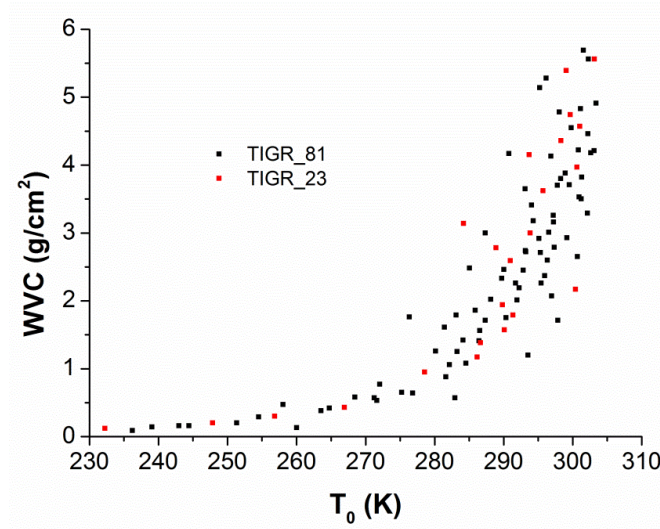
152

153 Figure 2. Distribution of in situ sea surface temperatures on the global ocean.

154 ***2.3 Atmospheric profile data***

155 Several sets of real atmospheric profiles, such as the Thermodynamic Initial
 156 Guess Retrieval (TIGR) database has been widely used for the development of
 157 SST and LST retrieval algorithms (Scott and Chédin 1981; Chédin et al. 1985).
 158 In this work, the TIGR database TIGR2002_v1.1 was used as input to the
 159 radiative transfer simulation (see Section 2.4). Due to the large size of the
 160 TIGR2002_v1.1 and concentrations of water vapor content (WVC) less than 1
 161 g/cm^2 , it is reasonable to select different atmospheric profiles according to well-
 162 distributed values of WVC. Figure 3 shows the 104 atmospheric profiles
 163 selected, with the atmospheric temperature in the lowest layer (T_0) varying from
 164 232.25 K to 303.41 K and the WVC from 0.09 g/cm^2 to 5.69 g/cm^2 , which
 165 constructed a robust database capable of representing global atmospheric
 166 conditions with a moderate number of samples and a nearly uniform WVC

167 distribution. Eighty-one profiles (referred to as TIGR_81) were used for
168 developing the SST retrieval algorithm and twenty-three profiles (referred to as
169 TIGR_23) were used for validation.



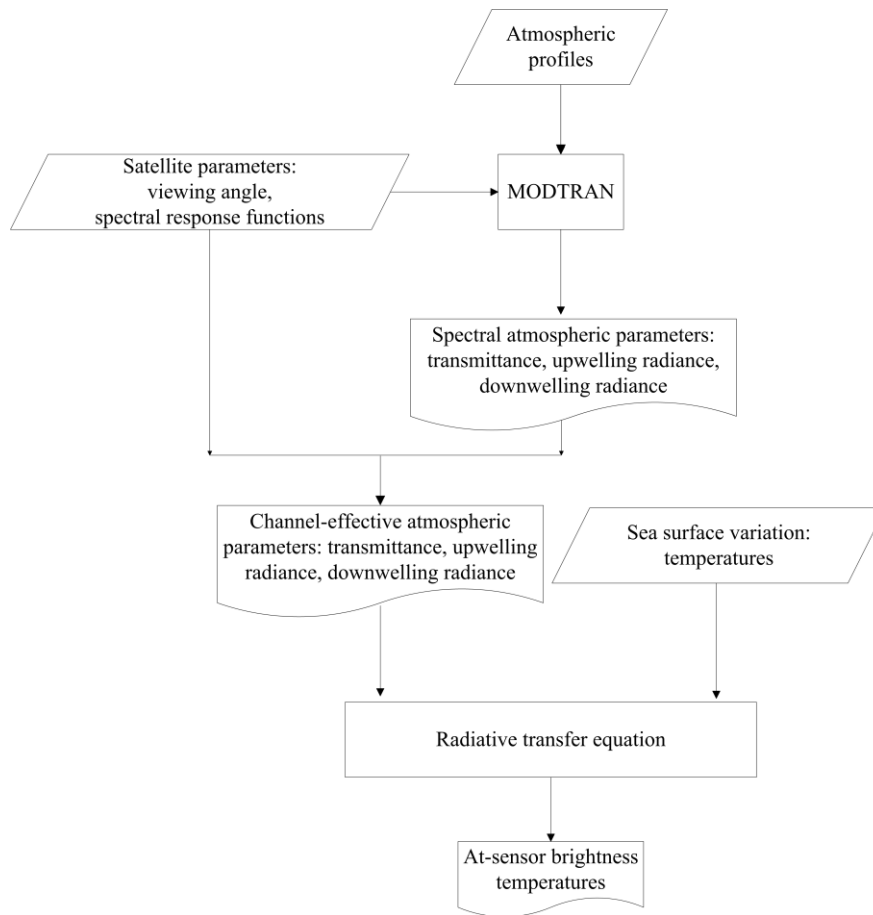
170

171 Figure 3. Plot of the total water vapor content (WVC) as a function of
172 atmospheric temperature in the lowest layer (T_0) for selected atmospheres.
173 TIGR_81 was used for algorithm development (black points) and TIGR_23
174 (red points) for algorithm validation.

175 **2.4 Generation of the simulated database**

176 To obtain an appropriate simulated database for developing a SST retrieval
177 algorithm for GF-5 TIR data, the atmospheric radiative transfer model
178 MODTRAN (Berk et al. 1999) was used to simulate the spectral atmospheric
179 parameters of spectral transmittance τ_λ , spectral atmospheric upwelling
180 radiance $R_{atm,\lambda}^\uparrow$ and spectral atmospheric downwelling $R_{atm,\lambda}^\downarrow$. The channel-
181 effective atmospheric parameters τ_i , $R_{atm,i}^\uparrow$ and $R_{atm,i}^\downarrow$ can be obtained by

182 integrating these spectral variables with spectral response functions in CH_{10.8}
183 and CH_{11.95}. The channel brightness temperature T_i at the top of the atmosphere
184 (TOA) can then be determined according to the radiative transfer equation
185 (RTE) (Coll and Caselles 1994; Niclòs et al. 2007) by inverting the Planck
186 function in combination with a wide range of SSTs, considering the VZA of 0°.
187 For a more realistic simulation, the SSTs reasonably vary with T_0 . Specifically,
188 five SSTs ($T_0 - 5$ K, $T_0 - 2$ K, T_0 K, $T_0 + 2$ K and $T_0 + 5$ K) were considered in
189 this study. All of the data were obtained considering the emissivity to be equal
190 to one because the ocean surface radiates almost as a blackbody at infrared
191 wavelengths (McClain, Pichel, and Walton 1985). A flow chart of generation
192 of the simulated data is presented in Figure 4.



193

194

Figure 4. The procedure of generating the simulated data.

195

3. Method of revising the linear SW algorithm

196

The theoretical basis for the SST retrieval algorithm relies on the RTE.

197

Assuming that: 1) the first-order Taylor approximation of the Planck function

198

was used and 2) the atmospheric equivalent temperatures in two TIR channels

199

were equal ($T_{ai} = T_{aj}$), a typical linear SW algorithm (Sobrino, Li, and Stoll

200

1993; McClain, Pichel, and Walton 1985; Barton 1995; Kilpatrick, Podestfi,

201

and Evans 2001) can be obtained:

202
$$T_s = T_i + A(T_i - T_j) \quad (1)$$

203 where T_s is the sea surface temperature (*i.e.*, SST; hereafter, SST is used
 204 interchangeably with T_s), T_i and T_j are the brightness temperatures in channels
 205 i and j at the TOA, and A is the coefficient defined by $A = (1 - \tau_i) / (\tau_i - \tau_j)$ in
 206 which τ_i and τ_j are the transmittances through the atmosphere from the surface
 207 to the satellite in channels i and j . Eq. (1) indicates that a linear relationship
 208 exists between $T_s - T_i$ and $T_i - T_j$. However, an empirical quadratic relationship
 209 was found when relating $T_s - T_i$ to $T_i - T_j$. Coll et al. (1994) proposed a quadratic
 210 SW equation but no physical interpretation. In the next section, we will
 211 investigate the derivation of the quadratic SW equation by re-examining the
 212 two assumptions and approximations mentioned above.

213 ***3.1 Revision of the linearization of the Planck function***

214 Based on the RTE, Eq. (2) can be obtained by using Taylor's expansion of the
 215 Planck function,

216
$$T_i = T_{ai} + \tau_i(T_s - T_{ai}) + \Delta T_i \quad (2)$$

217 where ΔT_i is the error in T_i caused by linearizing the Planck function. In the
 218 published literature, ΔT_i is small and always neglected (McClain, Pichel, and
 219 Walton 1985; Walton et al. 1998; Prabhakara, Dalu, and Kunde 1974). Using
 220 the simulated data, the calculated results of ΔT_i for CH_{10.8} and CH_{11.95} by Eq.

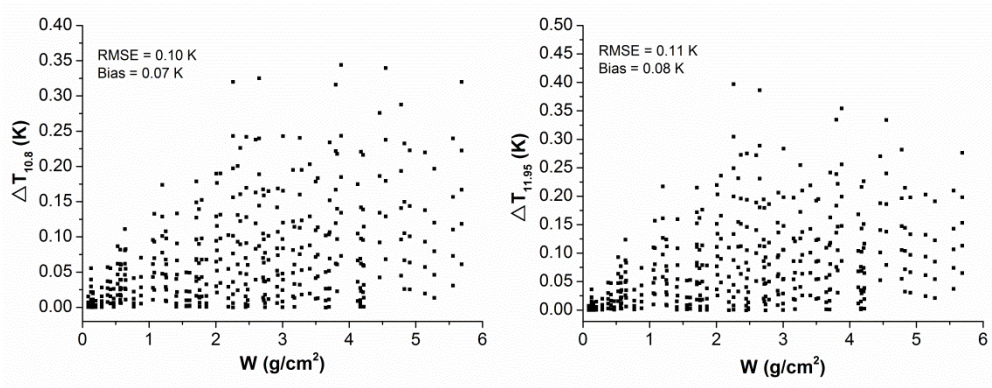
221 (2) are shown in Figure 5 (a) and (b). It can be observed that a RMSE of 0.10
 222 K and a bias of 0.07 K were obtained for CH_{10.8}, and those of CH_{11.95} were 0.11
 223 K and 0.08 K, respectively. Writing Eq. (2) for two channels, one can obtain
 224 Eq. (3),

$$225 \quad T_s = T_i + A(T_i - T_j) + \Delta T_{s1} + \Delta T_{s2} \quad (3)$$

226 where $\Delta T_{s1} = -\Delta T_i - A(\Delta T_i - \Delta T_j)$ with the same A as in Eq. (1), $\Delta T_{s2} = A_a(T_{ai}$
 227 $- T_{aj})$ with $A_a = -(1 - \tau_i)(1 - \tau_j) / (\tau_i - \tau_j)$. We can see that ΔT_{s1} is the error of T_s
 228 retrieval caused by linearizing the Planck function and ΔT_{s2} , which will be
 229 presented in Section 3.2, is the influence of the hypothesis $T_{ai} = T_{aj}$ on T_s
 230 retrieval. Figure 5 (c) displays the results of ΔT_{s1} , which is within the range of
 231 -0.4~0.5 K. The negative bias (-0.06 K) of ΔT_{s1} indicates that the surface
 232 temperature was overestimated due to the linearization of the Planck function,
 233 with RMSE = 0.10 K.

234

235

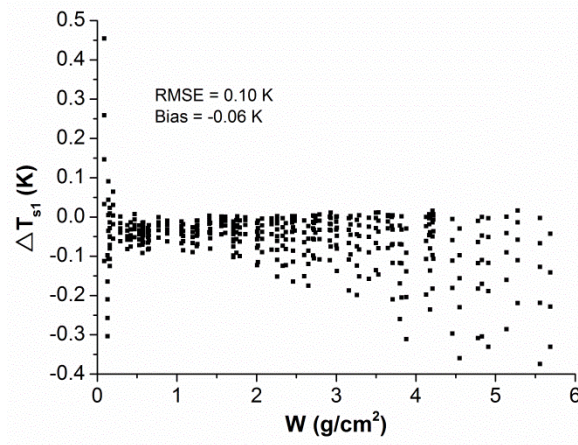


236

237

(a)

(b)



238

239

(c)

240 Figure 5. The error caused by the linearization of the Planck function for
 241 channels with central wavelengths of (a) 10.8 μm , (b) 11.95 μm and (c) for SST.

242 To revise the error caused by the linearization of the Planck function,
 243 the second-order derivative of Taylor's expansion was considered. Based on the
 244 RTE, ΔT_i in Eq. (2) can be rewritten as the following expression:

$$245 \quad \Delta T_i = \frac{\frac{1}{2} \left(\frac{\partial^2 B_i(T)}{\partial T^2} \right)_{T_i} [(1 - \tau_i)(T_{ai} - T_i)^2 + \tau_i(T_s - T_i)^2]}{\left(\frac{\partial B_i(T)}{\partial T} \right)_{T_i}} \quad (4)$$

246 where $(\frac{\partial B_i(T)}{\partial T})_{T_i}$ and $(\frac{\partial^2 B_i(T)}{\partial T^2})_{T_i}$ are the first-order and second-order
 247 derivatives of the Planck function at temperature T_i , respectively. Eq. (4) shows
 248 that ΔT_i is described by a complex expression. Parameterization of Eq. (4) is
 249 necessary. Considering the simplified case of Eq. (2) in which ΔT_i was
 250 regarded as zero, Eq. (2) can also be rewritten as:

$$251 \quad (1 - \tau_i)(T_i - T_{ai}) = \tau_i(T_s - T_i) \quad (5)$$

252 Putting the square on both sides of Eq. (5), one can obtain Eq. (6) by simple
 253 mathematical manipulation,

$$254 \quad (1 - \tau_i)(T_i - T_{ai})^2 = \tau_i(T_s - T_i)^2 \frac{\tau_i}{1 - \tau_i} \quad (6)$$

255 In addition, using the approximation of the Planck function in the work of Price
 256 (1984),

$$257 \quad B_i(T_i) = a_i T_i^{n_i} \quad (7)$$

258 where a_i and n_i are constants in a given channel, Eq. (8) can be obtained:

$$259 \quad (\frac{\partial^2 B_i(T)}{\partial T^2})_{T_i} / (\frac{\partial B_i(T)}{\partial T})_{T_i} = \frac{n_i - 1}{T_i} \quad (8)$$

260 Combining Eqs. (6) and (8), ΔT_i can be parameterized as $\frac{1}{2}(n_i - 1) \frac{(T_s - T_i)^2 \tau_i}{T_i(1 - \tau_i)}$.

261 As shown in Figure 6, there is a strong dependence between ΔT_i and

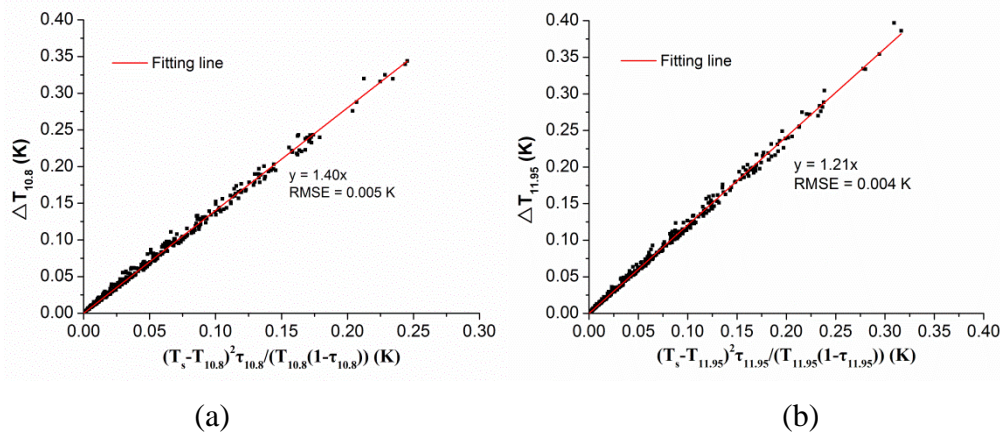
262 $\frac{(T_s - T_i)^2 \tau_i}{T_i(1 - \tau_i)}$, with sufficient accuracy of T_i (RMSE lower than 0.01 K) for both

263 channels. Based on Figure 6, ΔT_i is rewritten as:

264
$$\Delta T_i = \alpha_i \frac{(T_s - T_i)^2 \tau_i}{T_i(1 - \tau_i)} \quad (9)$$

265 where α_i is the regression coefficient, which is 1.40 for CH_{10.8} and 1.21 for

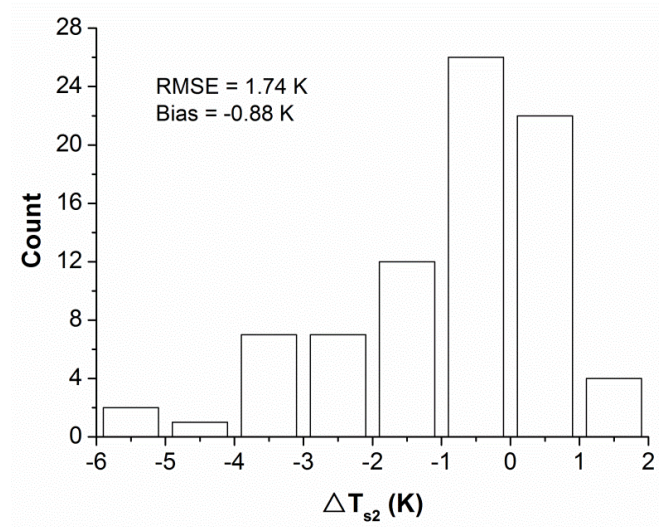
266 CH_{11.95}.



269 Figure 6. ΔT_i versus $(T_s - T_i)^2 \tau_i / (T_i (1 - \tau_i))$ for Gaofen-5 TIR channels
 270 centered at (a) 10.8 μm and (b) 11.95 μm . Here, T_s is the surface temperature,
 271 T_i is the simulated brightness temperature, τ_i is the transmittance and ΔT_i is the
 272 difference between the simulated and estimated brightness temperatures from
 273 Eq. (2).

274 **3.2 Revision of the $T_{ai} = T_{aj}$ hypothesis**

275 If the hypothesis of $T_{ai} = T_{aj}$ is used for the T_s retrieval, ΔT_{s2} in Eq. (3) is 0.
 276 However, according to the calculated $T_{a10.8}$ and $T_{a11.95}$ using the thermal-path
 277 atmospheric upwelling radiance generated from the simulation, ΔT_{s2} ranges
 278 from about -6~2 K, as seen in Figure 7. It can be concluded that use of the T_{ai}
 279 = T_{aj} hypothesis can lead to large error in T_s retrieval, with the RMSE of 1.74
 280 K and bias of -0.88 K.



281

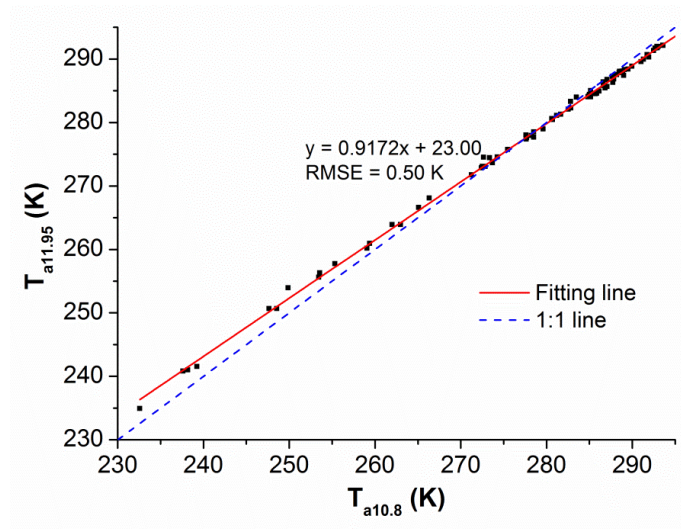
282 Figure 7. The error caused by the hypothesis of $T_{a10.8} = T_{a11.95}$ for SST retrieval.
 283 Here, $T_{a10.8}$ and $T_{a11.95}$ are the atmospheric equivalent temperatures in Gaofen-
 284 5 SW channels.

285 Notably, the discrepancy between T_{ai} and T_{aj} must be taken into account
 286 in SST retrieval from satellite observations (Franqois and Ottl é 1996). From
 287 Figure 8, it can be observed that 1) there is a discrepancy between $T_{a10.8}$ and
 288 $T_{a11.95}$ for GF-5 data, with $T_{a11.95} > T_{a10.8}$ for low $T_{a10.8}$ and $T_{a11.95} < T_{a10.8}$ for high
 289 $T_{a10.8}$. The maximum difference between $T_{a10.8}$ and $T_{a11.95}$ is almost 4 K; 2)
 290 $T_{a11.95}$ and $T_{a10.8}$ are approximately equal only in a small range of atmospheric

291 conditions, at approximately $T_{a10.8}$ between 275-285 K; 3) there is a linear
292 dependence between $T_{a10.8}$ and $T_{a11.95}$,

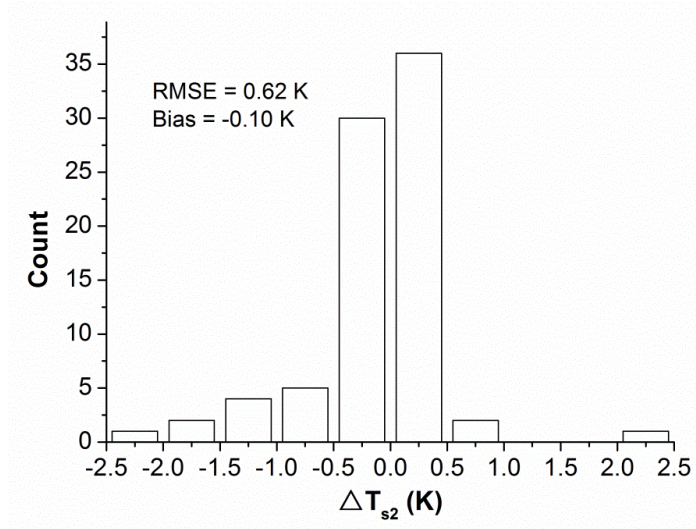
293
$$T_{a11.95} = aT_{a10.8} + b \quad (10)$$

294 where $a = 0.9172$ and $b = 23.00$, with RMSE = 0.50 K. Using this linear
295 relationship, the SST residual calculated by Eq. (3) is shown in Figure 9.
296 Compared with the result caused by the hypothesis of $T_{ai} = T_{aj}$, the RMSE is
297 changed to 0.62 K and the bias is changed to -0.10 K.



298

299 Figure 8. The relationship between atmospheric equivalent temperatures in two
300 Gaofen-5 TIR channels (labeled $T_{a10.8}$ and $T_{a11.95}$).



301

302 Figure 9. The SST residual obtained by Eq. (3) when the linear dependence of
 303 the atmospheric equivalent temperatures in two TIR channels was used.

304 Combining Eq. (9) and Eq. (10), the SST can be obtained by writing Eq.

305 (2) for two SW channels,

306
$$SST = MT_{10.8} + NT_{11.95} \quad (11)$$

307 where $M = \frac{A_4}{2(A_1 - A_2 \frac{T_{10.8}}{T_{11.95}})}$, $N = \frac{\sqrt{A_4^2 + 4(\frac{A_1}{T_{10.8}} - \frac{A_2}{T_{11.95}})(A_5 T_{10.8} + A_6 T_{11.95} + A_3)}}{2(A_1 \frac{T_{11.95}}{T_{10.8}} - A_2)}$,

308 with

309 $A_1 = \frac{a\alpha_{10.8}(1-\tau_{11.95})\tau_{10.8}}{1-\tau_{10.8}}$, $A_2 = \frac{\alpha_{11.95}(1-\tau_{10.8})\tau_{11.95}}{1-\tau_{11.95}}$, $A_3 = b(1-\tau_{10.8})(1-\tau_{11.95})$,

310 $A_4 = 2(A_1 - A_2) - a(1-\tau_{11.95})\tau_{10.8} + (1-\tau_{10.8})\tau_{11.95}$, $A_5 = -A_1 + a(1-\tau_{11.95})$,

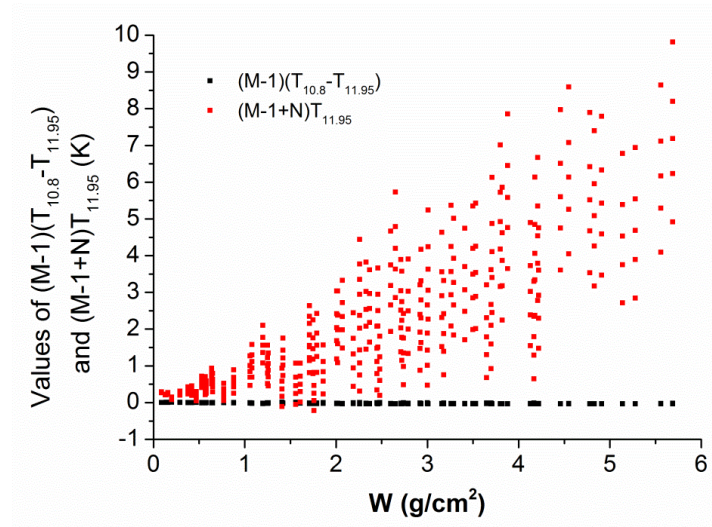
311 $A_6 = A_2 - (1-\tau_{10.8})$

312 **3.3 Analysis of the nonlinear SW algorithm**

313 Equation (11) is complex, requiring analysis and simplification. According to
 314 the simulated data, M ranged from 0.9620~0.9941 and N from 0.0328~0.0394.
 315 Taking the value of M approximately close to one, Eq. (11) can be rewritten as:

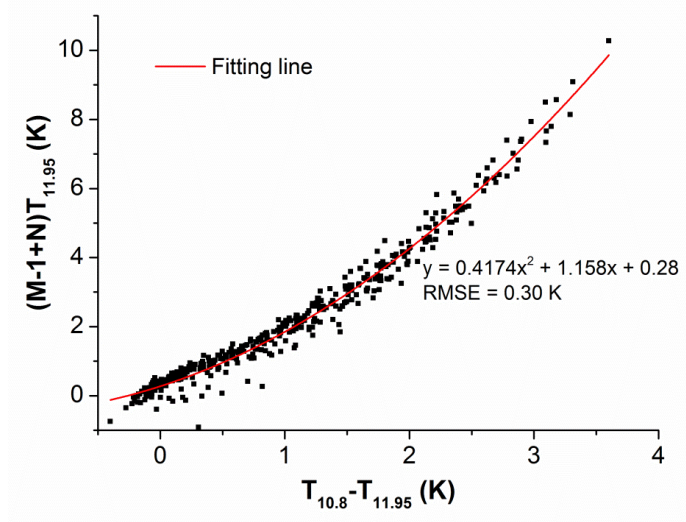
$$316 \quad SST - T_{10.8} = (M - 1)(T_{10.8} - T_{11.95}) + (M - 1 + N)T_{11.95} \quad (12)$$

317 Since $(M - 1)$ is close to 0, the first term of Eq. (12) (*i.e.*, $(M - 1)(T_{10.8} - T_{11.95})$)
 318 is small even if multiplied by the maximum of $(T_{10.8} - T_{11.95})$ (approximately 4
 319 K). In contrast to the small value of the first term, the second term (*i.e.*, $(M - 1$
 320 $+ N)T_{11.95}$) makes the main contribution to Eq. (12) (see Figure 10), because of
 321 the large value of $T_{11.95}$. Taking the structure of the SW algorithm into
 322 consideration, $(M - 1 + N)T_{11.95}$ should be the function of $(T_{10.8} - T_{11.95})$.
 323 Therefore, the relationship between $(M - 1 + N)T_{11.95}$ and $(T_{10.8} - T_{11.95})$ was
 324 investigated further. As shown in Figure 11, $(M - 1 + N)T_{11.95}$ can be
 325 parameterized using $(T_{10.8} - T_{11.95})$, with RMSE = 0.30 K.



326

327 Figure 10. Values of $(M - 1)(T_{10.8} - T_{11.95})$ and $(M - 1 + N)T_{11.95}$ in Eq. (12)
 328 versus the atmospheric water vapor content (WVC).



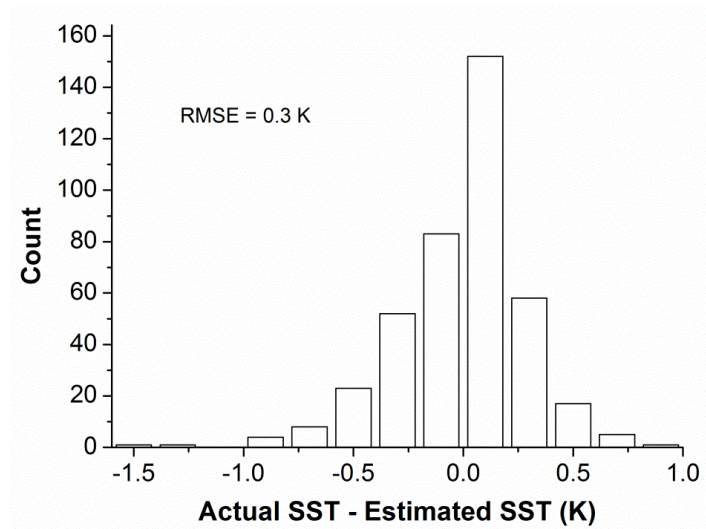
329

330 Figure 11. The relationship between $(M - 1 + N)T_{11.95}$ in Eq. (12) and the
 331 difference of the brightness temperatures in SW channels ($T_{10.8} - T_{11.95}$).

332 Based on the above analysis, Eq. (12) can be simplified as:

$$333 \quad SST - T_{10.8} = A(T_{10.8} - T_{11.95})^2 + B(T_{10.8} - T_{11.95}) + C \quad (13)$$

334 where A , B and C are the coefficients. Using the least-square fitting method, the
 335 coefficients $A = 0.4253$, $B = 1.123$ and $C = 0.28$ were obtained using the
 336 simulated data, with $RMSE = 0.30$ K. Figure 12 shows the histogram of the
 337 difference between the actual SST and that obtained by Eq. (13).



338

339 Figure 12. Histogram of the differences between the actual and estimated SSTs
 340 using Eq. (13).

341

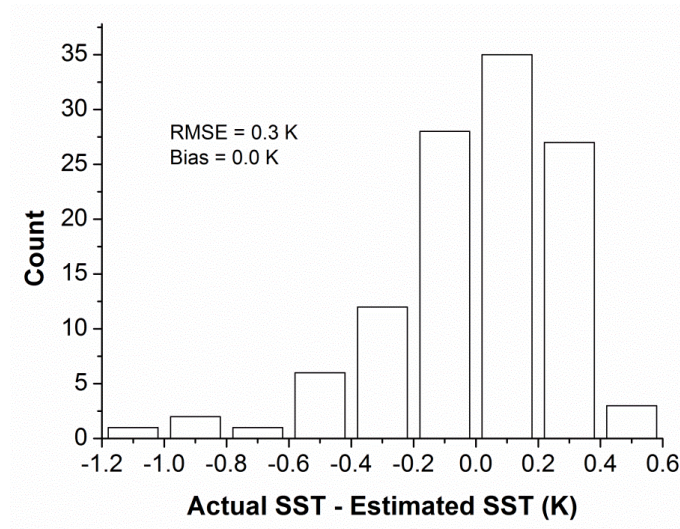
342 **4. Error analysis and validation**

343 *4.1 Error of the instrument noise*

344 The accuracy of the estimated SST will essentially depend on the radiometric
 345 performance of the instrument. The noise equivalent differential temperature
 346 (NE Δ T) in infrared channels is designed to be 0.2 K for GF-5 TIR data. To
 347 evaluate the performance of the quadratic algorithm in this study, a simulation
 348 of the effect of satellite noise was performed using a set of randomly generated
 349 signal level perturbations with errors of 0.1 K, 0.2 K and 0.3 K for both channels.
 350 The RMSEs between the true SSTs and those retrieved from the noise-added
 351 brightness temperatures are 0.49 K, 0.82 K and 1.20 K for NE Δ T = 0.1 K, 0.2
 352 K and 0.3 K, respectively, in both channels.

353 **4.2 Validation with simulated data**

354 To assess the general applicability of the quadratic SW equation to different
355 atmospheric conditions, the accuracy of Eq. (13) was also evaluated using
356 another set of data, TIGR_23. Figure 13 presents the error distribution between
357 the true and the estimated SSTs, with RMSE = 0.3 K and bias = 0 K.



358

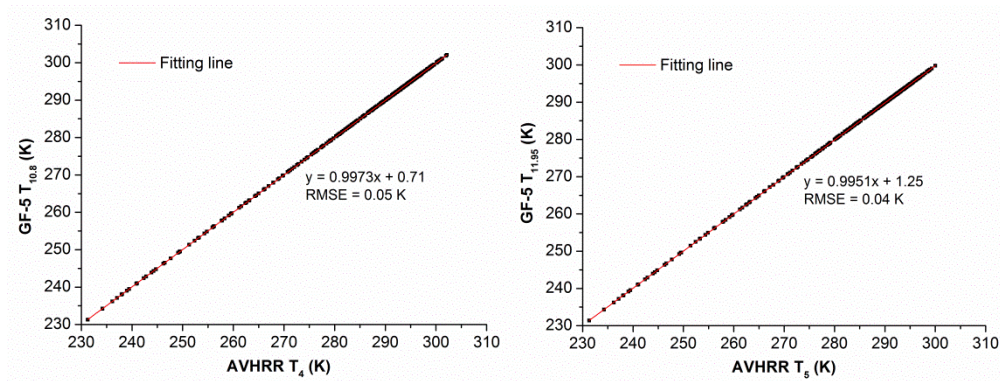
359 Figure 13. Histogram of the differences between the true and estimated SSTs
360 based on TIGR_23 data.

361 **4.3 Validation using Matchup dataset**

362 **4.3.1 Data processing**

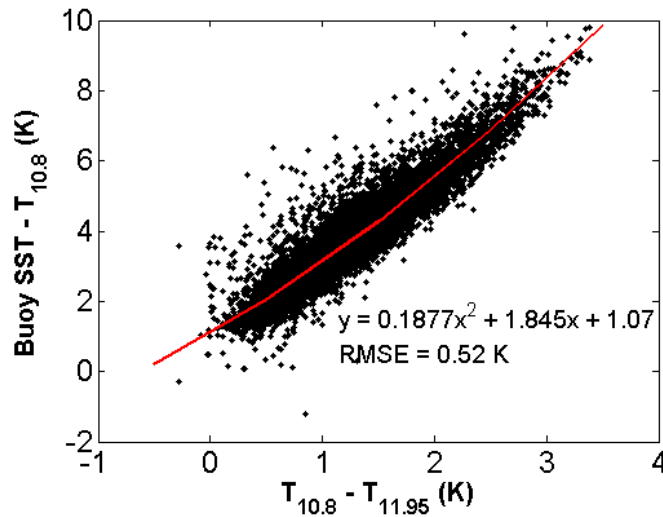
363 The invalid values in MDS were first cleaned out. Considering that MSI
364 instrument observes the earth almost at nadir, the data within the VZA of 20 °,
365 which contains 24231 pairs of in situ SSTs and AVHRR at-sensor brightness
366 temperatures matchup data, was used in this study. In order to get the “true”

367 GF-5/MSI brightness temperatures, the relationship between GF-5/MSI and
368 AVHRR brightness temperatures was established using the simulated data for
369 each SW channel, as presented in Figure 14. It can be seen that there is a strong
370 linear relationship between GF-5/MSI and AVHRR brightness temperatures
371 with the RMSE no higher than 0.05 K for both channels. Using this relationship,
372 the “real” GF-5/MSI at-sensor brightness temperatures can be calculated from
373 AVHRR brightness temperatures in MDS. 24231 pairs of in situ SSTs and
374 coincident in time and space GF-5/MSI brightness temperatures were then
375 established. It should be noted that simulations may be significantly biased with
376 respected to observations due to modeling errors and not fully accuracy
377 atmospheric profiles. Observed data is also affected by uncertainties in
378 calibration, spectral response functions and residual cloud. Therefore, the
379 algorithm coefficients based on the observed data is needed to retrieve SST
380 from GF-5 satellite data. Among 24231 pairs of in situ SSTs and GF-5/MSI
381 brightness temperatures matchup data, 10000 pairs were used to obtain the
382 algorithm coefficients suitable for GF-5/MSI data, while the remaining 14231
383 pairs were used for validation purpose. According to the Figure 15, which
384 presents the quadratic relationship between buoy SSTs and GF-5/MSI
385 brightness temperatures, the coefficients $A = 0.1877$, $B = 1.845$ and $C = 1.07$ in
386 the quadratic SW algorithm were obtained for GF-5/MSI data, with the RMSE
387 = 0.52 K.



388

389 Figure 14. Plot of the simulated AVHRR and GF-5/MSI brightness
 390 temperatures for each of split-window channel.



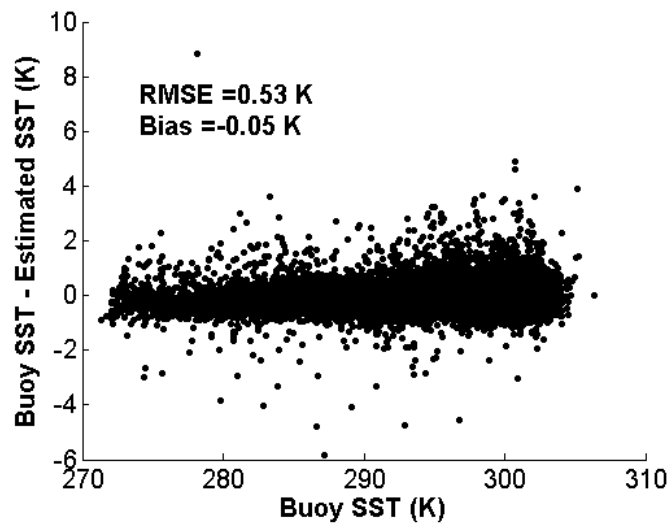
391

392 Figure 15. Plot of $(\text{Buoy SST} - T_{10.8})$ and $(T_{10.8} - T_{11.95})$. Here, Buoy SST is the
 393 sea surface temperature measured by drifting buoy, $T_{10.8}$ and $T_{11.95}$ are the GF-
 394 5/MSI brightness temperatures calculated from AVHRR brightness
 395 temperatures in MDS.

396 *4.3.2 Validation results*

397 Using the coefficients given in Section 4.3.1, SSTs were calculated from the
 398 remaining GF-5/MSI data. Analyzing comparisons of GF-5/MSI SSTs with

399 buoy SSTs gives a bias of -0.05 K and a RMSE of 0.53 K, as shown in Figure
400 16. Among the 14231 pairs data, 95.45% of the differences between buoy SSTs
401 and GF-5/MSI SSTs are within ± 1 K. From Figure 16, one may note that, there
402 is a large error up to about 8 K. This may be related to the contribution of some
403 materials floating on ocean or the incorrect measurement by accidental.



404
405 Figure 16. Buoy sea surface temperature minus sea surface temperature
406 obtained by GF-5/MSI.

407 5. Discussion

408 Although many studies report the quadratic SW algorithm, this study aims for
409 a well understanding of the semi-empirical quadratic SW algorithm. The
410 analyses were based on a comprehension of the derivation procedure of the
411 linear SW equation. The SST errors resulted from the linearization of the Planck
412 function were RMSE = 0.10 K and bias = -0.06 K, while the ones from the
413 hypothesis of $T_{ai} = T_{aj}$ were 1.74 K and -0.88 K. Although the influence of the

414 linearization of the Planck function on SST retrieval was not obvious as the
415 effect of the $T_{ai} = T_{aj}$ hypothesis, in order to interpret the physical derivation of
416 the quadratic SW algorithm, the second-order derivative of Taylor's expansion
417 of the Planck function and the linear dependence between atmospheric
418 equivalent temperatures in two SW channels were considered. The obtained
419 nonlinear SW algorithm by combining the two revisions of the Planck function
420 linearization and of the $T_{ai} = T_{aj}$ hypothesis is complex. However, it can be
421 simplified to the quadratic structure of $(T_i - T_j)$, meaning that the nonlinear SW
422 algorithm is equivalent to the quadratic SW equation. Compared with the
423 previous studies, which presented the quadratic relationship between TOA
424 brightness temperatures and the surface temperature by maintaining the
425 structure of linear SW algorithm but no physical interpretation, this study
426 makes the physical interpretation of the semi-empirical quadratic SW algorithm
427 clear theoretically and improves our understanding of the quadratic SW
428 algorithm.

429 **6. Conclusions**

430 Some assumptions and approximations were used in the derivation of the linear
431 SW equation. Using the simulated data, this work carefully evaluated these
432 assumptions and approximations based on the RTE. We found that these
433 assumptions and approximations were not precise for SST retrieval. Therefore,
434 the revised equations for the Planck function linearization and for the

435 relationship between the atmospheric equivalent temperatures in SW channels
436 of GF-5 data were created. Based on these studies, a nonlinear SW algorithm
437 was obtained. Further analysis of the nonlinear SW algorithm clarified that it is
438 equivalent to the quadratic SW equation but highlights the theoretical
439 interpretation.

440 The effects of instrument noise on SST retrieval using the developed
441 quadratic SW algorithm were analyzed. The total errors were 0.49 K, 0.82 K
442 and 1.20 K for NEΔTs of 0.1 K, 0.2 K and 0.3 K, respectively. The validation
443 using the MDS produced by EUMETSAT OSI-SAF presented a RMSE of 0.53
444 K and a bias of -0.05 K.

445 A GF-5 satellite carrying a MSI instrument with narrow swaths and a
446 high resolution of 40 meters is scheduled to be launched in 2017. The analysis
447 of GF-5 satellite data will be performed in future work when the data is
448 available. Because land surface is much more complicated than sea surface and
449 the LST differs significantly from the air temperature near the surface, large
450 errors may be introduced by the assumptions and approximations used in the
451 derivation of the linear SW method. This hypothesis will be tested in future
452 work.

453 **Funding**

454 National high-resolution earth observation project (11-Y20A32-9001-15/17).

455 **Acknowledgments**

456 Thanks are given to Professor Christopher Merchant in the University of
457 Reading, who provided the MDS.

458 **References**

- 459 Anding, D., and R. Kauth. 1970. "Estimation of sea surface temperature from
460 space." *Remote Sensing of Environment* 1:217-20.
- 461 Barnett, T. P., N. Graham, S. Pazan, W. White, M. Latif, and M. Flügel. 1993.
462 "ENSO and ENSO-related predictability. Part I: Prediction of
463 equatorial pacific sea surface temperature with a hybrid coupled
464 ocean–atmosphere model." *Journal of Climate* 6:1545-66.
- 465 Barton, I. J. 1983. "Dual channel satellite measurements of sea surface
466 temperature." *Quarterly Journal of the Royal Meteorological Society*
467 109 (460):365-78.
- 468 Barton, Ian J. 1995. "Satellite-derived sea surface temperatures: Current status."
469 *Journal of Geophysical Research* 100 (C5):8777-90. doi:
470 10.1029/95jc00365.
- 471 Becker, F. 1987. "The impact of spectral emissivity on the measurement of land
472 surface temperature from a satellite." *International Journal of Remote*
473 *Sensing* 8 (10):1509-22. doi: 10.1080/01431168708954793.
- 474 Becker, François, and Zhao-Liang Li. 1990. "Towards a local split window
475 method over land surfaces." *International Journal of Remote Sensing*
476 11 (3):369-93. doi: 10.1080/01431169008955028.
- 477 Berk, A., G.P. Anderson, P.K. Acharya, J.H. Chetwynd, L.S. Bernstein, E.P.
478 Shettle, M.W. Matthew, and S.M. Adler-Golden. 1999. "MODTRAN
479 4 user's manual." *MA: Air Force Reserach Laboratory, Hanscom AFB.*
- 480 Chédin, A., N.A. Scott, C. Wahiche, and P. Moulinier. 1985. "The improved
481 initialization inversion method: A high resolution physical method for
482 temperature retrievals from satellites of the TIROS-N series." *Journal*
483 *of Climate and Applied Meteorology* 24:128-43.
- 484 Chelton, Dudley B., and Frank J. Wentz. 2005. "Global microwave satellite
485 observations of sea surface temperature for numerical weather
486 prediction and climate research." *Bulletin of the American*
487 *Meteorological Society* 86 (8):1097-115. doi: 10.1175/bams-86-8-
488 1097.
- 489 Coll, César, and Vicente Caselles. 1997. "A split-window algorithm for land
490 surface temperature from advanced very high resolution radiometer
491 data: Validation and algorithm comparison." *Journal of Geophysical*

492 *Research: Atmospheres* 102 (D14):16697-713. doi:
493 10.1029/97jd00929.

494 Coll, C., and V. Caselles. 1994. "Analysis of the atmospheric and emissivity
495 influence on the splitwindow equation for sea surface temperature."
496 *International journal of remote sensing* 15 (9):1915-32. doi:
497 10.1080/01431169408954216.

498 Coll, C., V. Caselles, J. A. Sobrino, and E. Valor. 1994. "On the atmospheric
499 dependence of the split-window equation for land surface
500 temperature." *International Journal of Remote Sensing* 15 (1):105-22.
501 doi: 10.1080/01431169408954054.

502 Donlon, C., N. Rayner, I. Robinson, D. J. S. Poulter, K. S. Casey, J. Vazquez-
503 Cuervo, E. Armstrong, et al. 2007. "The global ocean data assimilation
504 experiment high-resolution sea surface temperature pilot project."
505 *Bulletin of the American Meteorological Society* 88 (8):1197-213. doi:
506 10.1175/bams-88-8-1197.

507 Fisher, Edwin L. 1958. "The exchange of energy between the sea and the
508 atmosphere in relation to hurricane behavior." *Journal of Meteorology*
509 15:164-71.

510 Francois, C., and C. Ottl é 1996. "Atmospheric corrections in the thermal
511 infrared: Global and water vapor dependent split-window algorithms-
512 Applications to ATSR and AVHRR data." *IEEE Transactions on*
513 *Geoscience and Remote Sensing* 34 (2):457-70.

514 Kilpatrick, K. A., G. P. Podestfi, and R. Evans. 2001. "Overview of the
515 NOAA/NASA advanced very high resolution radiometer Pathfinder
516 algorithm for sea surface temperature and associated matchup
517 database." *Journal of Geophysical Research* 106 (C5):9179-97.

518 Liu, Yang, and Peter J. Minnett. 2015. "Evidence linking satellite-derived sea-
519 surface temperature signals to changes in the Atlantic meridional
520 overturning circulation." *Remote Sensing of Environment* 169:150-62.
521 doi: 10.1016/j.rse.2015.08.014.

522 Liu, Z.-L., H. Wu, B.-H. Tang, S. Qiu, and Z.-L. Li. 2013. "Atmospheric
523 corrections of passive microwave data for estimating land surface
524 temperature." *Optics express* 21 (13):15654-63. doi:
525 10.1364/OE.21.015654.

526 McClain, E. Paul, William G. Pichel, and Charles C. Walton. 1985.
527 "Comparative performance of AVHRR-based multichannel sea surface
528 temperatures." *Journal of Geophysical Research* 90 (C6):11587. doi:
529 10.1029/JC090iC06p11587.

530 McMillin, L.M. . 1975. "Estimation of sea surface temperature from two
531 infrared window measurements with different absorption." *Journal of*
532 *Geophysical Research* 80 (36):5113-7.

533 Niçòs, Raquel, Vicente Caselles, César Coll, and Enric Valor. 2007.
534 "Determination of sea surface temperature at large observation angles

535 using an angular and emissivity-dependent split-window equation."
536 *Remote Sensing of Environment* 111 (1):107-21. doi:
537 10.1016/j.rse.2007.03.014.

538 Petrenko, Boris, Alexander Ignatov, Yury Kihai, John Stroup, and Prasanjit
539 Dash. 2014. "Evaluation and selection of SST regression algorithms for
540 JPSS VIIRS." *Journal of Geophysical Research: Atmospheres* 119
541 (8):4580-99. doi: 10.1002/2013jd020637.

542 Pinardi, N., I. Allen, E. Demirov, P. De Mey, G. Korres, A. Lascaratos, P.-Y.
543 Le Traon, C. Maillard, G. Manzella, and C. Tziavos. 2003. "The
544 Mediterranean ocean forecasting system first phase of implementation
545 (1998-2001)." *Annales Geophysicae* 21 (1):3-20.

546 Prabhakara, C., G. Dalu, and V.G. Kunde. 1974. "Estimation of sea surface
547 temperature from remote sensing in the 11-13 μ m window region."
548 *Journal of Geophysical Research* 79:5039-44.

549 Qian, Y.-G., N. Wang, L.-L. Ma, Y.-K. Liu, H. Wu, B.-H. Tang, L.-L. Tang,
550 and C.-R. Li. 2016. "Land surface temperature retrieved from airborne
551 multispectral scanner mid-infrared and thermal-infrared data." *Optics*
552 *express* 24 (2):A257-69. doi: 10.1364/OE.24.00A257.

553 Rozenstein, O., Z. Qin, Y. Derimian, and A. Karnieli. 2014. "Derivation of land
554 surface temperature for Landsat-8 TIRS using a split window
555 algorithm." *Sensors (Basel)* 14 (4):5768-80. doi: 10.3390/s140405768.

556 Scott, N.A., and A. Chédin. 1981. "A fast line-by-line method for atmospheric
557 absorption computations: The Automatized Atmospheric Absorption
558 Atlas." *Journal of Applied Meteorology* 20:802-12.

559 Simpson, James J. 1994. "Remote sensing in fisheries: A tool for better
560 management in the utilization of a renewable resource." *Canadian*
561 *Journal of Fisheries and Aquatic Sciences* 51:743-71.

562 Sobrino, J.A., C. Coll, and V. Caselles. 1991. "Atmospheric corrections for land
563 surface temperature using AVHRR channels 4 and 5." *Remote Sensing*
564 *of Environment* 38:19-34.

565 Sobrino, José A., Zhao-Liang Li, and Marc P. Stoll. 1993. "Impact of the
566 atmospheric transmittance and total water vapor content in the
567 algorithms for estimating satellite sea surface temperatures." *IEEE*
568 *Transactions on Geoscience and Remote Sensing* 31 (5):946-52.

569 Ulivieri, C., M. M. Castronuovo, R. Francioni, and A. CardiUo. 1994. "A split
570 window algorithm for estimating land surface temperature from
571 satellites." *Advances in Space Research* 14 (3):59-65.

572 Walton, C. C., W. G. Pichel, J. F. Sapper, and D. A. May. 1998. "The
573 development and operational application of nonlinear algorithms for
574 the measurement of sea surface temperatures with the NOAA polar-
575 orbiting environmental satellites." *Journal of Geophysical Research:*
576 *Oceans* 103 (C12):27999-8012. doi: 10.1029/98jc02370.

577